MATERIALS SCIENCE

High n-type and p-type conductivities and power factors achieved in a single conjugated polymer

Zi-Di Yu[1], Yang Lu[1], Zi-Yuan Wang[1], Hio-Ieng Un[2], Szymon J. Zelewski[2,3], Ying Cui[4], Hao-Yang You[1], Yi Liu[1], Ke-Feng Xie[4], Ze-Fan Yao[1], Yu-Cheng He[4], Jie-Yu Wang[1], Wen-Bing Hu[4], Henning Sirringhaus[2], Jian Pei[1]*

The charge transport properties of conjugated polymers are commonly limited by the energetic disorder. Recently, several amorphous conjugated polymers with planar backbone conformations and low energetic disorder have been investigated for applications in field-effect transistors and thermoelectrics. However, there is a lack of strategy to finely tune the interchain π-π contacts of these polymers that severely restricts the energetic disorder of interchain charge transport. Here, we demonstrate that it is feasible to achieve excellent conductivity and thermoelectric performance in polymers based on thiophene-fused benzodifurandione oligo(*p*-phenylenevinylene) through reducing the crystallization rate of side chains and, in this way, carefully controlling the degree of interchain π-π contacts. N-type (p-type) conductivities of more than 100 S cm^{-1} (400 S cm^{-1}) and power factors of more than 200 μW m^{-1} K^{-2} (100 μW m^{-1} K^{-2}) were achieved within a single polymer doped by different dopants. It further demonstrated the state-of-the-art power output of the first flexible single-polymer thermoelectric generator.

INTRODUCTION

The emergence of conjugated polymers enables a new generation of flexible and wearable electronic devices that can be realized by solution processing (*1*–*4*). Most recently, with a deeper understanding of conjugated polymers, the performance of polymer (semi-)conductor devices has been notably improved (*5*–*11*); however, their relatively poor charge transport property is still insufficient to support a wide range of practical applications. The insufficiency of charge transport in polymer films is mainly attributed to the large energetic disorder caused by the inhomogeneous structural disorder of polymer films (*12*–*19*). Because of high energetic disorder resulting in barriers for charge transport, a thermally activated charge transport behavior has been observed in most conjugated polymers (*20*–*26*). In doped systems, the introduced molecular dopants provide an additional source of disorder as they can distort molecular conformations and disrupt the molecular packing in conjugated polymers (*27*–*30*). Thus, it is still challenging to achieve efficient charge transport in doped conjugated polymers.

One reported approach to decreasing energetic disorder for charge transport has been to design rigid rod–conjugated polymers that exhibited a uniform, ideally planar chain conformation with minimum variations in torsion angles along the polymer backbone (*31*, *32*). In this family of polymers, which are often not very crystalline, high carrier mobilities have been reported in field-effect transistors. Recently, they have also been explored for other applications, such as thermoelectrics, that require high mobilities to be maintained in films that are doped in their bulk to high carrier concentrations >10^{19} to 10^{21} cm^{-3}. In a family of such rigid-rod, planar copolymers based on thiophene-fused benzodifurandione oligo(*p*-phenylenevinylene) (TBDOPV), we recently demonstrated that high n-type electrical conductivities and excellent thermoelectric performance were achieved even though the polymer is only weakly crystalline. A weakly crystalline microstructure facilitated a high miscibility with molecular dopants and permitted high doping levels, while in systems with more crystalline microstructures, conductivity can be limited by dopant incorporation (*33*, *34*). The high performance of such weakly crystalline polymers can be attributed to the fast charge transport along the polymer backbone, but the presence of some degree of π-π contacts between the conjugated backbones remain important to facilitate efficient interchain charge transport. This may not require extended crystallites, but a careful control of π-π interactions is crucial in such polymers to optimize charge transport properties. The ability of the backbones to form such π-π contacts is affected by the crystallization behavior of the long alkyl side chains, which account for more than 50 weight % of the polymer and, in some cases, solidify at room temperature (fig. S2). Restraining the rapid crystallization behavior of the side chains may be an effective strategy to encourage the formation of π-π contacts and to further improve the charge transport properties.

Here, we report a facile approach to carefully control π-π contacts between adjacent main chains in the best-performing thiophene-based TBDOPV copolymer (TBDOPV-T) identified in our previous study (*33*, *34*) by reducing the crystallization rate of the alkyl side chains. Three different branched side chains with the branching points located one, three, and five carbon atoms away from the backbone, named TBDOPV-T-118, TBDOPV-T-318, and TBDOPV-T-518, were developed as illustrated in Fig. 1A. Photothermal deflection spectroscopy (PDS) provides solid evidence that TBDOPV-T-518 achieves the smallest energetic disorder at

[1]Beijing National Laboratory for Molecular Sciences (BNLMS), Key Laboratory of Polymer Chemistry and Physics of Ministry of Education, Center of Soft Matter Science and Engineering, College of Chemistry and Molecular Engineering, Peking University, Beijing 100871, China. [2]Optoelectronics Group, Cavendish Laboratory, University of Cambridge, JJ Thomson Avenue, Cambridge CB3 0HE, UK. [3]Department of Semiconductor Materials Engineering, Faculty of Fundamental Problems of Technology, Wrocław University of Science and Technology, Wybrzeże Wyspiańskiego 27, Wrocław 50-370, Poland. [4]Department of Polymer Science and Engineering, State Key Lab of Coordination Chemistry, School of Chemistry and Chemical Engineering, Nanjing University, Nanjing 210023, China.
*Corresponding author. Email: jianpei@pku.edu.cn

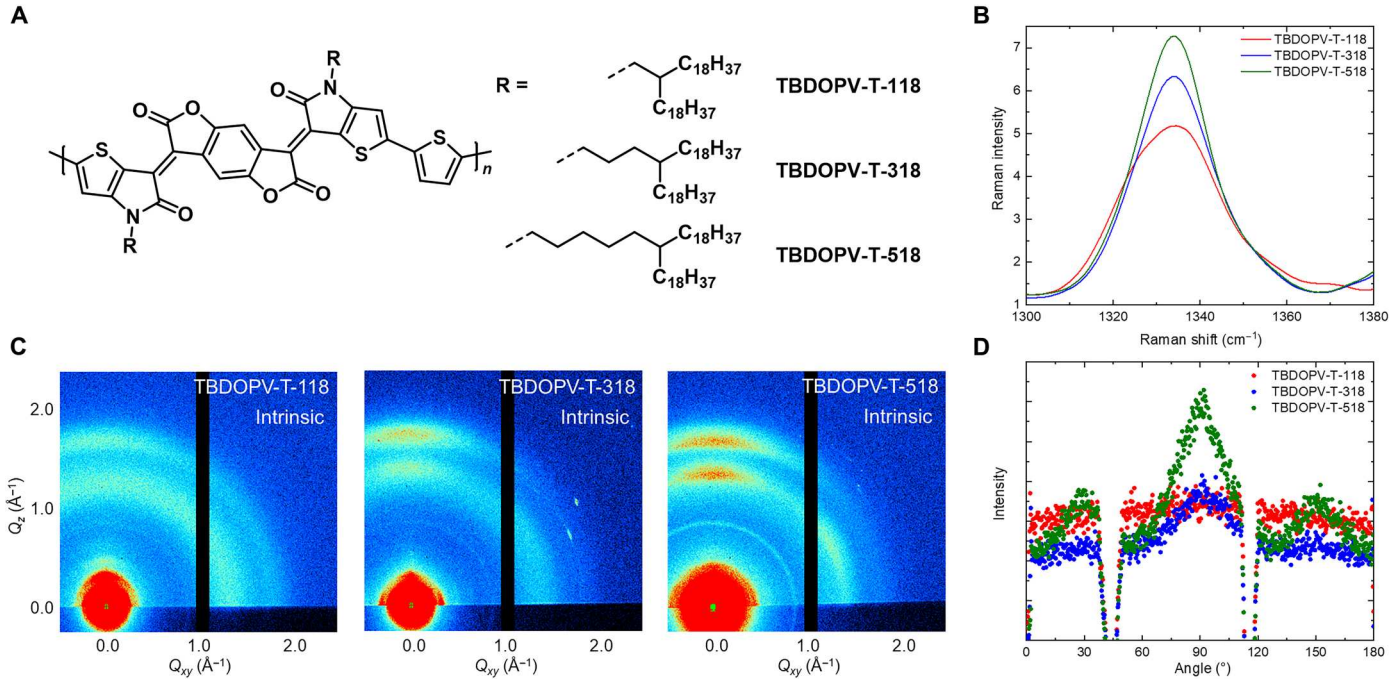

Fig. 1. Solid-state microstructures. (**A**) Chemical structures of TBDOPV-T–based polymers with different side chains. (**B**) Raman spectra from 1300 to 1380 cm^{-1} of intrinsic films of these three TBDOPV-T polymers. The peak intensity is normalized by the peak at around 1750 cm^{-1}. (**C**) GIWAXS patterns of intrinsic thick films of these three polymers. (**D**) Integrated intensity plots azimuthally along the ring at Q_r approximate to 1.5 $Å^{-1}$ (for TBDOPV-T-518 and TBDOPV-T-318) and 1.4 $Å^{-1}$ (for TBDOPV-T-118).

room temperature with the enhanced formation of π-π contacts. A nearly temperature-independent conductivity in doped TBDOPV-T-518 was observed near room temperature, indicating an ideal barrier-free transport. After doping with different dopants, TBDOPV-T-518 showed both high n-type and p-type conductivities. An n-type conductivity of 114 S cm^{-1} was reached with 4-(1,3-dimethyl-2,3-dihydro-1*H*-benzimidazol-2-yl)phenyl)dimethylamine (*N*-DMBI) and a p-type conductivity of 452 S cm^{-1} was reached with $FeCl_3$. Furthermore, a relatively high Seebeck coefficient was also achieved, leading to high power factors for both types (more than 200 μW m^{-1} K^{-2} for n-type and more than 100 μW m^{-1} K^{-2} for p-type). Last, the first single-polymer flexible thermoelectric device was fabricated with the record power output up to 404 nW, in which *N*-DMBI–doped TBDOPV-T-518 was used as n-legs and $FeCl_3$-doped TBDOPV-T-518 was used as p-legs.

RESULTS

Grazing-incidence wide-angle x-ray scattering (GIWAXS) was performed to explore the microstructures of intrinsic films of these three polymers. All films exhibited a stacking diffraction signal at Q_r = 1.82 $Å^{-1}$ along the Q_z axis, suggesting the existence of face-on–oriented crystallites (Fig. 1C). As the branching positions of alkyl chains move outward, a decrease in π-π distance might be expected. However, this phenomenon was not that apparent for these TBDOPV-T polymers: π-π distances are 3.47 Å for TBDOPV-T-518 and TBDOPV-T-318, and 3.50 Å for TBDOPV-T-118 (fig. S5). Instead, a gradually enhanced intensity of the π-stacking diffraction was observed, indicating an increase in fraction, which is likely to be conducive to improving charge transport between adjacent chains. The diffraction signal at $Q_r \approx 1.5$ $Å^{-1}$ from the lamellar side-chain packing shows an anisotropic distribution in TBDOPV-T-518 (Fig. 1D), providing evidence for a bimodal face-on/edge-on distribution of the crystallites. By contrast, the diffraction signal in TBDOPV-T-118 is broader and more isotropic, suggesting more disorder in the packing of the alkyl side chains, which may be mainly responsible for the weaker π stacking. Consistently, the atomic force microscopy image of the TBDOPV-T-518 film (details in Materials and Methods and the Supplementary Materials) showed more nanoaggregates and a rougher surface.

The solution absorption spectroscopy of these three polymers behaves similarly (fig. S8), which is understandable as they share the same conjugated backbone. The solvation effect leads to a relatively free extension of polymer chains in solution, resulting in similar spectroscopic properties in solution. In films, the characteristic peak in the Raman spectrum of TBDOPV-T-518 at 1336 cm^{-1} (representing the stretching vibration of the conjugated backbone) showed a subtle narrowing compared to those of the other two polymers (Fig. 1B and further details in Materials and Methods and the Supplementary Materials). A similar difference was also found in the absorption spectrum (fig. S8) of TBDOPV-T-518 as a slight narrowing of the dominant absorption peak at around 1200 nm. These results imply a possible lower energetic disorder for the TBDOPV-T-518 film. These subtle differences in the spectroscopic properties of the films are consistent with the increased π-stacking diffraction in the GIWAXS and reflect the better ability of the chains to pack orderly when the branching points are moved outward.

To better understand the effect of alkyl side chain on π-π stacking, fast scanning calorimetry (*35*) was used to characterize the melting behaviors of these three polymers. The polymer samples

were annealed at temperatures ranging from −75° to 125°C for 1-s crystallization before a heating scan with a scan rate of 8000 K s^{-1} to monitor the melting process (Fig. 2) (*36*, *37*). Each curve in Fig. 2A demonstrates the melting peak after annealing at 125°C, and TBDOPV-T-518 showed the lowest melting temperature, which was mainly ascribed to the side chains. The annealing temperatures affected the melting processes mainly in the range from −75° to 45°C, as shown by the high-temperature melting peaks in Fig. 2B (further details in Materials and Methods and the Supplementary Materials). TBDOPV-T-518 exhibited the weakest temperature dependence of melting enthalpy (Fig. 2C), suggesting the slowest crystallization rate owing to the weakest thermodynamic driving forces. On the basis of the above results, it was supposed that the crystallization rate of side chains may affect the stacking of the conjugated backbones in the deposition of polymer films. For TBDOPV-T-118, the fast crystallization rate of side chains may make the disordered entanglement of the side chains take precedence over the stacking of the backbone, hindering the formation of effective π-contacts; however, for TBDOPV-T-518, the slow crystallization rate of side chains enables the conjugated fragments to form π stacking with a face-on orientation first, and the ordered π stacking and slow crystallization rate of side chains may induce the formation of ordered anisotropic arrangement of side chains shown in GIWAXS (Fig. 1D).

In light of this, we speculate that the stacking of conjugated backbone is mainly formed in solvent volatilization for these weakly crystalline polymers, which usually have an excellent solubility (*32*). A slower crystallization rate of side chains is expected not to interfere with the orderly stacking of the backbone (*38*). In brief, by reducing the crystallization rate of side chains, the π-π stacking was enhanced in these TBDOPV-T polymers. As stated above, the control of crystallization of side chains is expected to be crucial for achieving optimum charge transport in such weakly crystalline polymers.

The Seebeck coefficient α was measured as a function of doping level in films that were n-type doped using *N*-DMBI. We first conducted measurements in a regime of relatively low doping levels ($n < 7 \times 10^{19}$ cm^{-3}). A reduction of the Seebeck coefficient with increasing doping level was observed, which became weaker the further the branching point was removed from the backbone (Fig. 3A) (*23*, *32*, *39*). For the interpretation of these data, a model assumed that the energetic disorder is less than the thermal energy k_BT among transport sites and that all the transport sites are thermally accessible (*17*–*19*). For small carrier concentration, the Seebeck coefficient α is mainly contributed by the change of the system's entropy produced by adding a charge carrier and can be expressed as (for n-type) (*17*)

$$\alpha = -\left[\frac{k_B}{e}\ln\left(\frac{N - n_c}{n_c}\right) + \frac{k_B}{e}\ln(2) + \alpha_{vib}\right] \quad (1)$$

where N is the density of thermally accessible sites, and n_c is the density of mobile carriers. The three terms refer to changes in the entropy of mixing, the spin entropy, and the vibrational entropy upon adding a charge carrier. A fraction $1 - f$ can be introduced as the ratio of the effective mobile electron concentration n and the added dopant concentration: $1 - f = n_c/n(N\text{-DMBI})$, where $n(N\text{-DMBI})$ is the density of *N*-DMBI in films. At a low doping level ($N >> n_c$)

$$\alpha = -\left\{\frac{k_B}{e}\ln\left[\frac{N}{n(N - \text{DMBI})(1 - f)}\right] + \frac{k_B}{e}\ln(2) + \alpha_{vib}\right\} \quad (2)$$

$$\alpha = -\left\{\frac{k_B}{e}\ln[2N/n(N - \text{DMBI})] + A\right\} \quad (3)$$

$$A = -\frac{k_B}{e}\ln(1 - f) + \alpha_{vib} \quad (4)$$

The fraction f takes into account that not all charge carriers are free to contribute to the conduction and the Seebeck voltage but may reside in trap states as a result of residual energetic disorder and/or a reduced doping efficiency due to Coulombic trapping by the dopant counterions. To evaluate the change of Seebeck coefficient, we estimated N_0 by assuming that there is one transport site on each polymer repeat unit. On this premise, we obtained $N_0 = 3.5 \times 10^{20}$ cm^{-3} for TBDOPV-T-518, 3.6×10^{20} cm^{-3} for TBDOPV-T-318, and 3.7×10^{20} cm^{-3} for TBDOPV-T-118. The dashed line is a plot of $\alpha = -(k_B/e)\ln[2N_0/n(N\text{-DMBI})]$, expressed as a straight line in the logarithmic diagram (Fig. 3A).

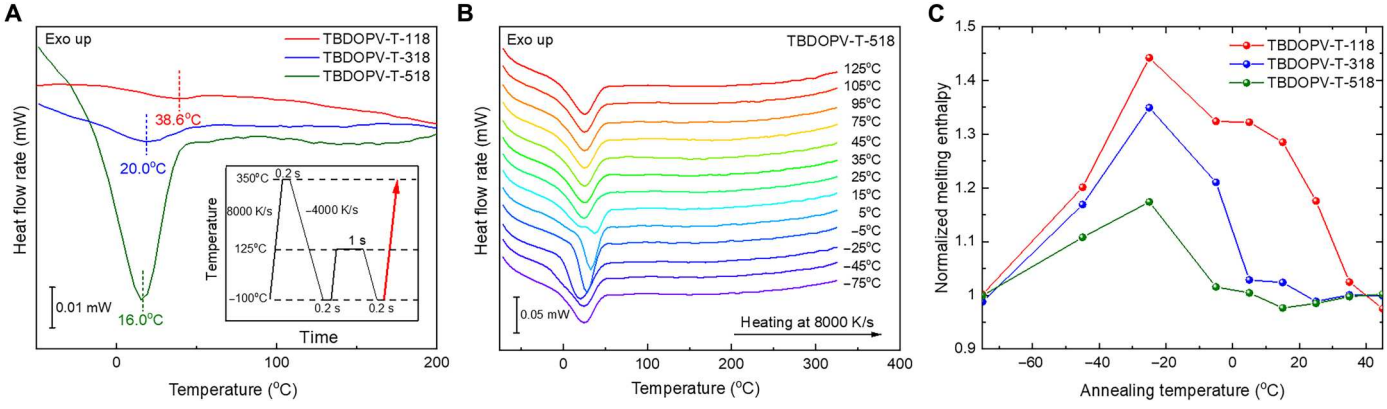

Fig. 2. Flash differential scanning calorimetry of three TBDOPV-Ts. (**A**) Heat flow scans of TBDOPV-T-118, TBDOPV-T-318, and TBDOPV-T-518 films during fast heating with 8000 K s^{-1} after aging at 125°C for 1 s as the inset scheme of temperature protocols. (**B**) Heat flow scans of TBDOPV-T-518 films during fast heating after aging at various temperatures as labeled. (**C**) Melting enthalpy of the split high-temperature peaks for three TBDOPV-T films at temperatures from −75° to 45°C.

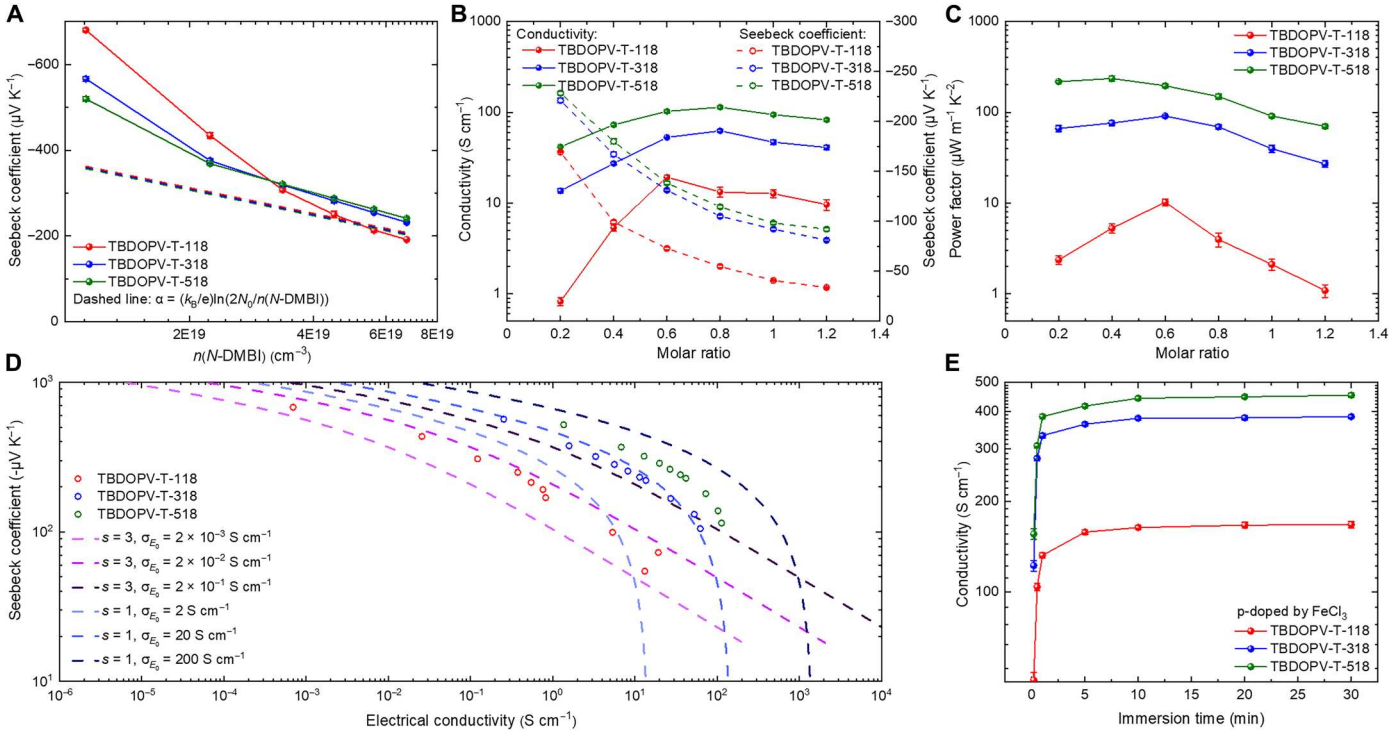

Fig. 3. The density of thermally accessible sites, conductivity, and thermoelectric performance. (**A**) Seebeck coefficients of *N*-DMBI–doped TBDOPV-T polymer films at low doping level. The gray dashed line is the plot of $\alpha = -k_B/e \ln[2\ N/n(N\text{-DMBI})]$. (**B**) Dopant fraction–dependent conductivity and Seebeck coefficients of *N*-DMBI–doped TBDOPV-T polymer films. (**C**) Dopant fraction–dependent power factors of *N*-DMBI–doped TBDOPV-T polymer films. (**D**) Kang-Snyder model fitting. The dashed lines are calculated with the parameters given in the figure. (**E**) Conductivity of $FeCl_3$-doped TBDOPV-T polymer films [molar ratio = *n*(dopant)/*n*(repeat units of polymer)].

The difference between the trend of the experimental data and the dashed line is attributed to reductions in *f*, i.e., filling of trap states, as *n*(*N*-DMBI) increases. As a result, the slopes for the three polymers are gradually approaching the ideal, trap-free slope indicated by the dashed line. Among these three polymers, the slope for TBDOPV-T-518 remains closest to the dashed line at a low doping level, which implies fewer traps. With the increase of doping level, these three polymers exhibited a change in the relative order of the magnitude of their Seebeck coefficients. TBDOPV-T-518 showed the highest Seebeck coefficient among these polymers. Within the model, this can be attributed to different values of *N* (according to Eq. 3), and the higher Seebeck coefficient of TBDOPV-T-518 (absolute value) therefore indicated a higher density of thermally accessible sites and a lower degree of energetic disorder.

N-DMBI–doped TBDOPV-T-518 films exhibited a higher n-type conductivity up to 114 S cm^{-1} alongside its higher Seebeck coefficient (Fig. 3B). The simultaneous improvement of conductivity and Seebeck coefficient enabled an exceptionally high power factor of 200 μW m^{-1} K^{-2} for an n-type polymer thermoelectric material (Fig. 3C). Compared to the common approach of adjusting the carrier concentration, which could only balance conductivity and Seebeck coefficient (*40*), the apparent increase of the density of thermally accessible sites observed here resulted in a simultaneous improvement of conductivity and Seebeck coefficient, which improved the thermoelectric performance significantly. It was also found that when an $FeCl_3$ solution was used to p-dope TBDOPV-T-518 films by immersion doping, a high conductivity of more than 400 S cm^{-1} and a power factor of more than 100 μW m^{-1} K^{-2} were obtained (Fig. 3E and fig. S20).

To further explore the charge transport characteristics of these three conjugated polymers, the Kang-Snyder model was used to analyze the α-σ relationship (Fig. 3D) (*24*). This model expresses the energy-dependent conductivity function as a power law with an exponent *s*, which characterizes the transport physics and density of states of the doped conjugated polymer. It was observed to better fit the α-σ curve of TBDOPV-T-518 with $s = 1$ than $s = 3$. An exponent $s = 3$ is expected if the dominant scattering of the charge carriers is by ionized impurities, while $s = 1$ could be interpreted as indicating that charge transport is dominated by acoustic-phonon scattering (*24*). While other interpretations of the exponent are possible, it is important to note that another polymer semiconductor, for which $s = 1$ has been reported, is PEDOT, which is one of the best p-type conductive materials (*24*). Within the Kang-Snyder model, the prefactor of the energy-dependent conductivity σ_{E0} was fitted as about 50 S cm^{-1} for doped TBDOPV-T-518, which was close to that of PEDOT:tosylate (75 S cm^{-1}) (*24*).

The temperature-dependent electrical conductivities of the doped polymers with maximum σ were measured (Fig. 4A) from 300 to 400 K. The doped TBDOPV-T-518 films showed a near temperature-independent transport behavior implying a barrier-free transport with a negligible degree of energetic disorder, while for the other two polymers, the conductivity increased with increasing temperature. This was achieved in films processed just by solution doping, i.e., mixing the dopant into the polymer solution. Below 300 K, the conductivities of doped TBDOPV-T-518 films decreased

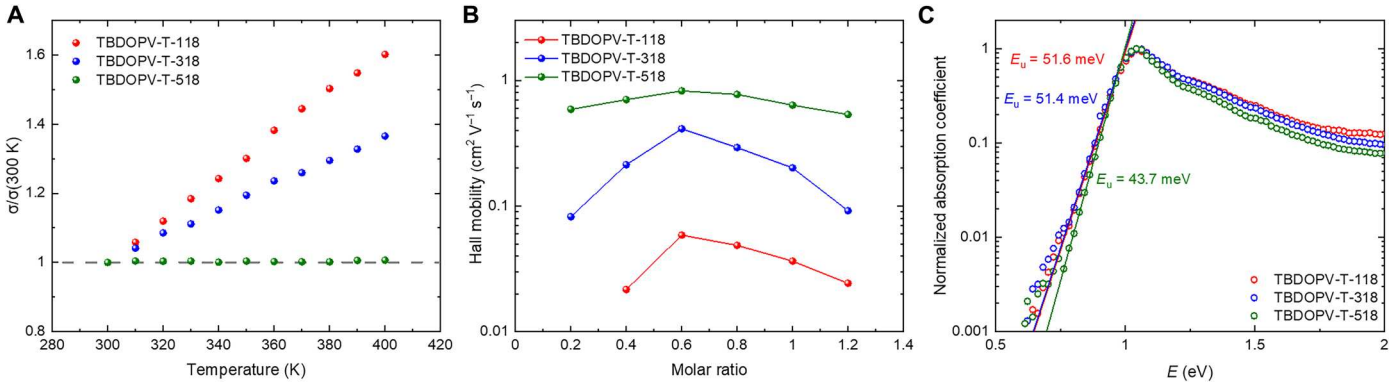

Fig. 4. Charge transport behavior and energetic disorder. (**A**) Temperature-dependent electrical conductivity of *N*-DMBI–doped TBDOPV-T polymer films. (**B**) Hall mobilities of *N*-DMBI–doped TBDOPV-T polymer films [molar ratio = *n*(dopant)/*n*(repeat units of polymer)]. (**C**) Normalized absorption coefficient of these three TBDOPV-T polymer films, measured by PDS.

as the temperature dropped (fig. S22) but less strongly than for the other polymers. This is likely due to residual energetic disorder. As the thermal energy k_BT reduces, the energetic dispersion gradually becomes nonnegligible and starts to limit the charge transport. Fitting an Arrhenius relationship from 100 to 300 K, a low activation energy of 11 meV was extracted for doped TBDOPV-T-518, which was less than k_BT at room temperature (25 meV).

AC Hall effect measurements were also performed, enhanced Hall mobilities approaching 1 $cm^2\ V^{-1}\ s^{-1}$ were observed in doped TBDOPV-T-518 (Fig. 4B), and nearly identical Hall carrier concentrations in the range between 2×10^{20} and $8 \times 10^{20}\ cm^{-3}$ (depending on doping concentration) were obtained in these three polymers (fig. S26). While the values of Hall carrier concentrations and mobilities are likely to be over-/underestimated, respectively, because of the effect of localized carriers that do not contribute to generating the Hall voltage but contribute to screening it (*41*), these measurements confirmed the similar doping degree of these three polymers. Extensive spectroscopic and chemical characterization of the films was performed, including optical absorption spectroscopy after doping, x-ray photoelectron spectroscopy, ultraviolet photoelectron spectroscopy, and electron spin resonance (further details in Materials and Methods and the Supplementary Materials). All these results suggested that the performance difference of the three polymers after doping was not due to different

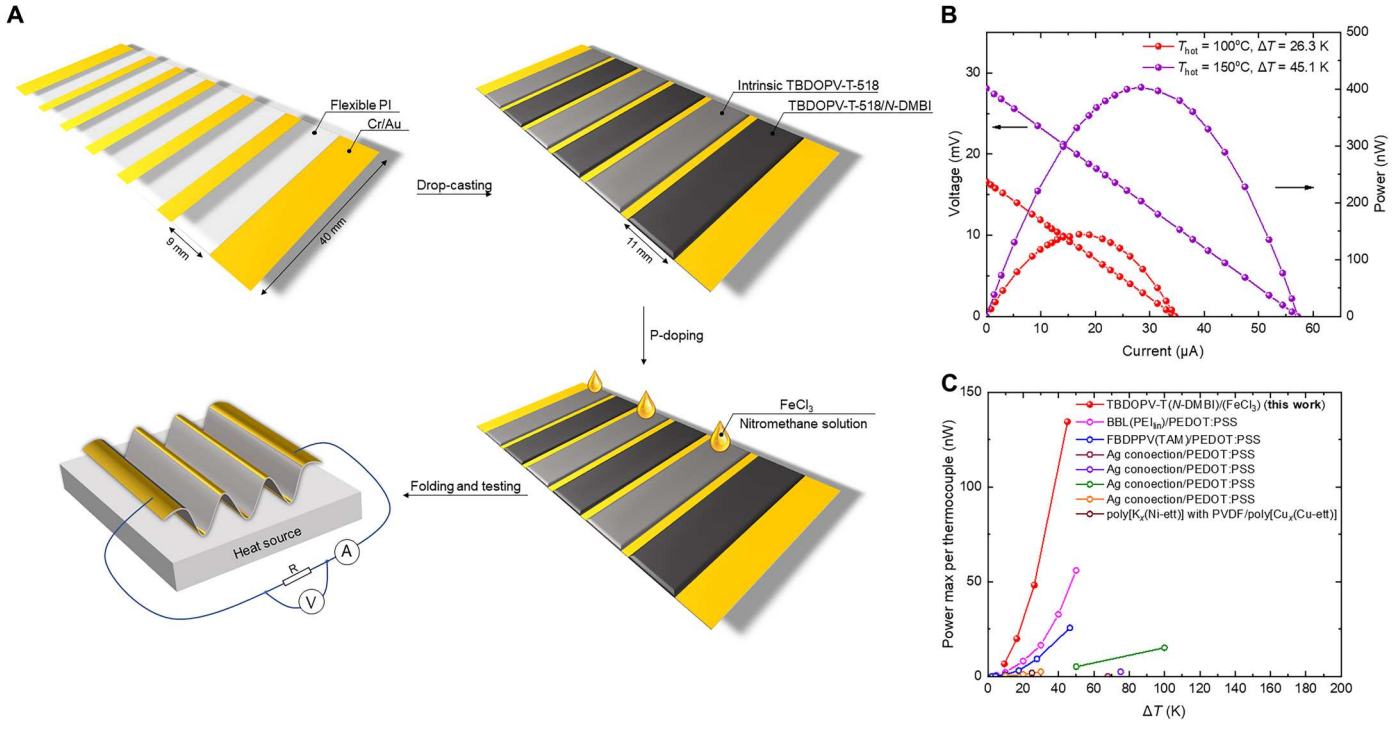

Fig. 5. Flexible single-polymer solution–processed thermoelectric generator. (**A**) Fabrication and testing of the single-polymer flexible thermoelectric generator (TEG). (**B**) Output voltage and power of the generator at different temperature differences. (**C**) Comparison of power output per module of polymer TEGs (*42*–*48*).

doping levels but due to the underpinning charge transport properties and the energetic disorder of the polymers.

PDS was used to characterize the degree of energetic disorder in these TBDOPV-T polymers in their undoped state (Fig. 4C). This technique provides a measurement of the energetic width of the sub-bandgap tail states of the excitonic joint density of states characterized by the Urbach energy, E_u (*32*). The Urbach energy was extracted from the optical absorption coefficient in the vicinity of the bandgap (Fig. 4C). TBDOPV-T-518 showed the lowest E_u (43.7 meV) among these three polymers, representing the smallest energy disorder. This is fully consistent with the more pronounced π-π stacking and the improved charge transport properties of TBDOPV-T-518.

The high thermoelectric performance of doped TBDOPV-T-518 for both n-type and p-type operation enables us to fabricate the first flexible organic thermoelectric generator (TEG) based on just a single thermoelectric material for both p-type and n-type legs. TBDOPV-T-518 films, which were n-doped by depositing from a solution containing *N*-DMBI and p-doped by immersion in $FeCl_3$ dissolved in nitromethane, were used as n-leg and p-leg materials, respectively. A flexible colorless polyimide (CPI) film was used as the substrate and provided a flexible support for the device. The fabrication process of the TEG is shown in Fig. 5A. First, the gold electrodes were patterned on CPI by evaporation through a mask. Then, TBDOPV-T-518/*N*-DMBI and intrinsic TBDOPV-T-518 were printed through drop-casting. Last, $FeCl_3$ solution was coated on the intrinsic TBDOPV-T-518 for p-doping and was removed after a 3-min immersion. The device was folded into a corrugated shape and was tested on a heated stage in air (further details in Materials and Methods and the Supplementary Materials). The internal resistance of the device was about 400 ohms. An open-circuit voltage of 28.1 mV and a short-circuit current of 57.2 μA were obtained while the stage was heated to 150°C (with temperature difference ΔT = 45.1 K), resulting in a maximum power output up to 404 nW (Fig. 5B). The power output per thermocouple showed the highest value for reported polymer TEGs, even though the same polymer was used for both n-type and p-type legs (Fig. 5C). In addition, the normalized maximum power output to describe the performance of thermoelectric devices (fig. S34) was evaluated. The normalized maximum power output for our thermoelectric device was calculated as 30.2 mW m^{-1}, 50 times higher than the value for FBDPPV:TAM/PEDOT:PSS (*42*).

DISCUSSION

Our results have provided a new perspective for achieving excellent conductivity and high thermoelectric performance in weakly crystalline rigid rod–conjugated polymers with planar backbone conformations. To make optimum use of the fast intrachain transport in these polymers, it is important to carefully control the degree of π-π contacts to achieve efficient interchain transport while maintaining the ability to dope these polymers to high doping concentrations. We have demonstrated that this can be achieved through a weaker crystallization rate of the alkyl side chains and adjusting the position of the branching point with respect to the main chain. This enables the conjugated backbone to spontaneously form π-π contacts during solution-deposition and annealing and achieve a low degree of energetic disorder and a high density of thermally accessible sites. In this way, we have been able to demonstrate conductivities of more than 100 S cm^{-1} and very high thermoelectric performance for both n-type and p-type operations. Our insights into the thermoelectric structure-property relationships of these polymers will hopefully stimulate the development of a new generation of high-performance planar, rigid rod–conjugated polymers for thermoelectric and other applications.

MATERIALS AND METHODS

Materials

N-DMBI was synthesized following the procedures from literature (*27*). TBDOPV-T-118 [M_n = 26.8 kDa and polymer dispersity index (PDI) = 4.04], TBDOPV-T-318 (M_n = 26.0 kDa and PDI = 3.79), and TBDOPV-T-518 (M_n = 29.0 kDa and PDI = 3.71) were synthesized following the procedures from literature (*31*) and are also shown in the Supplementary Materials.

Single-polymer TEG

The 10-μm-thick CPI substrate was purchased from NINGBO BOYA POLY ADVANCED MATERIALS CO. LTD. The CPI substrate was cleaned with isopropanol, dried with nitrogen, and then cleaned by plasma cleaning for 10 min. The 100-nm parallel gold electrodes along with 2 nm of the chromium adhesion layer were vacuum-evaporated to the substrate with mask. Then, the substrate was cleaned by plasma for another 10 min. Intrinsic TBDOPV-T-518 and *N*-DMBI–doped TBDOPV-T-518 were printed by drop-casting, respectively, and annealed at 120°C for 8 hours under nitrogen atmosphere. The three n-legs were packed by Kapton adhesive tape. The intrinsic films were doped by immersing in $FeCl_3$ nitromethane solution.

Photothermal deflection spectroscopy

PDS was performed using a tunable light source consisting of a 250-W quartz tungsten halogen lamp coupled to a 250-mm focal length grating monochromator. The monochromatic excitation beam was modulated with a mechanical chopper at 13 Hz and focused on the sample surface at normal incidence angle. The samples were immersed in FluorinertTM FC-72 (3M) liquid to improve the thermooptic response in the excitation spot surroundings. Thermal gradient at the sample surface caused by nonradiative relaxation caused deflection of a probe laser beam passed parallel to the sample surface (transverse configuration), detected by a quadrant photodiode and demodulated with a lock-in amplifier (Stanford Research Systems, SR830). The sub-gap (E_g) absorption data $A(E)$ were fitted to the Urbach formula assuming linear dependence of the PDS signal on the optical absorption coefficient, leading to determination of the Urbach energy (E_u) representing the electronic disorder

$$A\ (E) = \alpha_0 \exp\left(\frac{E - E_g}{E_u}\right)$$

Supplementary Materials

This PDF file includes:

Supplementary Text
Figs. S1 to S34
Tables S1 to S3
References

REFERENCES AND NOTES

1. Y. Wang, C. Zhu, R. Pfattner, H. Yan, L. Jin, S. Chen, F. Molina-Lopez, F. Lissel, J. Liu, N. I. Rabiah, Z. Chen, J. W. Chung, C. Linder, M. F. Toney, B. Murmann, Z. Bao, A highly stretchable, transparent, and conductive polymer. *Sci. Adv.* **3**, e1602076 (2017).
2. A. J. Heeger, Semiconducting polymers: The third generation. *Chem. Soc. Rev.* **39**, 2354–2371 (2010).
3. C. Wang, H. Dong, W. Hu, Y. Liu, D. Zhu, Semiconducting π-conjugated systems in field-effect transistors: A material odyssey of organic electronics. *Chem. Rev.* **112**, 2208–2267 (2012).
4. K. Xu, H. Sun, T.-P. Ruoko, G. Wang, R. Kroon, N. B. Kolhe, Y. Puttisong, X. Liu, D. Fazzi, K. Shibata, C.-Y. Yang, N. Sun, G. Persson, A. B. Yankovich, E. Olsson, H. Yoshida, W. M. Chen, M. Fahlman, M. Kemerink, S. A. Jenekhe, C. Muller, M. Berggren, S. Fabiano, Ground-state electron transfer in all-polymer donor-acceptor heterojunctions. *Nat. Mater.* **19**, 738–744 (2020).
5. K. Kang, S. Watanabe, K. Broch, A. Sepe, A. Brown, I. Nasrallah, M. Nikolka, Z. Fei, M. Heeney, D. Matsumoto, K. Marumoto, H. Tanaka, S.-I. Kuroda, H. Sirringhaus, 2D coherent charge transport in highly ordered conducting polymers doped by solid state diffusion. *Nat. Mater.* **15**, 896–902 (2016).
6. S. N. Patel, A. M. Glaudell, K. A. Peterson, E. M. Thomas, K. A. O'Hara, E. Lim, M. L. Chabinyc, Morphology controls the thermoelectric power factor of a doped semiconducting polymer. *Sci. Adv.* **3**, e1700434 (2017).
7. F. Zhang, C. A. Di, Exploring thermoelectric materials from high mobility organic semiconductors. *Chem. Mater.* **32**, 2688–2702 (2020).
8. Y. Lu, J.-Y. Wang, J. Pei, Strategies to enhance the conductivity of n-type polymer thermoelectric materials. *Chem. Mater.* **31**, 6412–6423 (2019).
9. T. Zhang, F. Wang, H.-B. Kim, I.-W. Choi, C. Wang, E. Cho, R. Konefal, Y. Puttisong, K. Terado, L. Kobera, M. Chen, M. Yang, S. Bai, B. Yang, J. Suo, S.-C. Yang, X. Liu, X. Fu, H. Yoshida, W. M. Chen, J. Brus, V. Coropceanu, A. Hagfeldt, J.-L. Brédas, M. Fahlman, D. S. Kim, Z. Hu, F. Gao, Ion-modulated radical doping of spiro-OMeTAD for more efficient and stable perovskite solar cells. *Science* **377**, 495–501 (2022).
10. H. Tang, Y. Liang, C. Liu, Z. Hu, Y. Deng, H. Guo, Z.-D. Yu, A. Song, H. Zhao, D. Zhao, Y. Zhang, X. Guo, J. Pei, Y. Ma, Y. Cao, F. Huang, A solution-processed n-type conducting polymer with ultrahigh conductivity. *Nature* **611**, 271–277 (2022).
11. H. Guo, C.-Y. Yang, X. Zhang, A. Motta, K. Feng, Y. Xia, Y. Shi, Z. Wu, K. Yang, J. Chen, Q. Liao, Y. Tang, H. Sun, H. Y. Woo, S. Fabiano, A. Facchetti, X. Guo, Transition metal-catalysed molecular n-doping of organic semiconductors. *Nature* **599**, 67–73 (2021).
12. K. Yang, X. Zhang, A. Harbuzaru, L. Wang, Y. Wang, C. Koh, H. Guo, Y. Shi, J. Chen, H. Sun, K. Feng, M. C. R. Delgado, H. Y. Woo, R. P. Ortiz, X. Guo, Stable organic diradicals based on fused quinoidal oligothiophene imides with high electrical conductivity. *J. Am. Chem. Soc.* **142**, 4329–4340 (2020).
13. Y. Lu, Z.-D. Yu, Y. Liu, Y.-F. Ding, C.-Y. Yang, Z.-F. Yao, Z.-Y. Wang, H.-Y. You, X.-F. Cheng, B. Tang, J.-Y. Wang, J. Pei, The critical role of dopant cations in electrical conductivity and thermoelectric performance of n-doped polymers. *J. Am. Chem. Soc.* **142**, 15340–15348 (2020).
14. Y.-Y. Zhou, Z.-Y. Wang, Z.-F. Yao, Z.-D. Yu, Y. Lu, X.-Y. Wang, Y. Liu, Q.-Y. Li, L. Zou, J.-Y. Wang, J. Pei, Systematic investigation of solution-state aggregation effect on electrical conductivity in doped conjugated polymers. *CCS Chem.* **3**, 2994–3004 (2021).
15. J. Bisquert, Interpretation of electron diffusion coefficient in organic and inorganic semiconductors with broad distributions of states. *Phys. Chem. Chem. Phys.* **10**, 3175–3194 (2008).
16. B. D. Naab, S. Guo, S. Olthof, E. G. Evans, P. Wei, G. L. Millhauser, A. Kahn, S. Barlow, S. R. Marder, Z. Bao, Mechanistic study on the solution-phase n-doping of 1,3-dimethyl-2-aryl-2,3-dihydro-1*H*-benzoimidazole derivatives. *J. Am. Chem. Soc.* **135**, 15018–15025 (2013).
17. D. Emin, Enhanced Seebeck coefficient from carrier-induced vibrational softening. *Phys. Rev. B* **59**, 6205–6210 (1999).
18. D. Huang, H. Yao, Y. Cui, Y. Zou, F. Zhang, C. Wang, H. Shen, W. Jin, J. Zhu, Y. Diao, W. Xu, C.-a. Di, D. Zhu, Conjugated-backbone effect of organic small molecules for n-type thermoelectric materials with *ZT* over 0.2. *J. Am. Chem. Soc.* **139**, 13013–13023 (2017).
19. M. Oehzelt, K. Akaike, N. Koch, G. Heime, Energy-level alignment at organic heterointerfaces. *Sci. Adv.* **1**, e1501127 (2015).
20. K. Lee, S. Cho, S. H. Park, A. J. Heeger, C.-W. Lee, S.-H. Lee, Metallic transport in polyaniline. *Nature* **441**, 65–68 (2006).
21. O. Bubnova, Z. U. Khan, H. Wang, S. Braun, D. R. Evans, M. Fabretto, P. H. Talemi, D. Dagnelund, J.-B. Arlin, Y. H. Geerts, S. Desbief, D. W. Breiby, J. W. Andreasen, R. Lazzaroni, W. M. Chen, I. Zozoulenko, M. Fahlman, P. J. Murphy, M. Berggren, X. Crispin, Semi-metallic polymers. *Nat. Mater.* **13**, 190–194 (2014).
22. D. Liu, J. Mun, G. Chen, N. J. Schuster, W. Wang, Y. Zheng, S. Nikzad, J.-C. Lai, Y. Wu, D. Zhong, Y. Lin, Y. Lei, Y. Chen, S. Gam, J. W. Chung, Y. Yun, J. B.-H. Tok, Z. Bao, A design strategy for intrinsically stretchable high-performance polymer semiconductors: Incorporating conjugated rigid fused-rings with bulky side groups. *J. Am. Chem. Soc.* **143**, 11679–11689 (2021).
23. W. C. Germs, K. Guo, R. A. J. Janssen, M. Kemerink, Unusual thermoelectric behavior indicating a hopping to bandlike transport transition in pentacene. *Phys. Rev. Lett.* **109**, 016601 (2012).
24. S. D. Kang, G. J. Snyder, Charge-transport model for conducting polymers. *Nat. Mater.* **16**, 252–257 (2017).
25. S. A. Gregory, R. Hanus, A. Atassi, J. M. Rinehart, J. P. Wooding, A. K. Menon, M. D. Losego, G. J. Snyder, S. K. Yee, Quantifying charge carrier localization in chemically doped semiconducting polymers. *Nat. Mater.* **20**, 1414–1421 (2021).
26. A. L. Efros, B. I. Shklovskii, Coulomb gap and low temperature conductivity of disordered systems. *J. Phys. C: Solid State Phys.* **8**, 49–51 (1975).
27. I. Salzmann, G. Heimel, M. Oehzelt, S. Winkler, N. Koch, Molecular electrical doping of organic semiconductors: Fundamental mechanisms and emerging dopant design rules. *Acc. Chem. Res.* **49**, 370–378 (2016).
28. J. Liu, Y. Shi, J. Dong, M. I. Nugraha, X. Qiu, M. Su, R. C. Chiechi, D. Baran, G. Portale, X. Guo, L. J. Koster, A., Overcoming coulomb interaction improves free-charge generation and thermoelectric properties for n-doped conjugated polymers. *ACS Energy Lett.* **4**, 1556–1564 (2019).
29. J. E. Cochran, M. J. N. Junk, A. M. Glaudell, P. L. Miller, J. S. Cowart, M. F. Toney, C. J. Hawker, B. F. Chmelka, M. L. Chabinyc, Molecular interactions and ordering in electrically doped polymers: Blends of PBTTT and F_4TCNQ. *Macromolecules* **47**, 6836–6846 (2014).
30. R. A. Schlitz, F. G. Brunetti, A. M. Glaudell, P. L. Miller, M. A. Brady, C. J. Takacs, C. J. Hawker, M. L. Chabinyc, Solubility-limited extrinsic n-type doping of a high electron mobility polymer for thermoelectric applications. *Adv. Mater.* **26**, 2825–2830 (2014).
31. T. H. Thomas, D. J. Harkin, A. J. Gillett, V. Lemaur, M. Nikolka, A. Sadhanala, J. M. Richter, J. Armitage, H. Chen, I. McCulloch, S. M. Menke, Y. Olivier, D. Beljonne, H. Sirringhaus, Short contacts between chains enhancing luminescence quantum yields and carrier mobilities in conjugated copolymers. *Nat. Commun.* **10**, 2614 (2019).
32. D. Venkateshvaran, M. Nikolka, A. Sadhanala, V. Lemaur, M. Zelazny, M. Kepa, M. Hurhangee, A. J. Kronemeijer, V. Pecunia, I. Nasrallah, I. Romanov, K. Broch, I. McCulloch, D. Emin, Y. Olivier, J. Cornil, D. Beljonne, H. Sirringhaus, Approaching disorder-free transport in high-mobility conjugated polymers. *Nature* **515**, 384–388 (2014).
33. Y. Lu, Z.-D. Yu, H.-I. Un, Z.-F. Yao, H.-Y. You, W. Jin, L. Li, Z.-Y. Wang, B.-W. Dong, S. Barlow, E. Longhi, C. Di, D. Zhu, J.-Y. Wang, C. Silva, S. R. Marder, J. Pei, Persistent conjugated backbone and disordered lamellar packing impart polymers with efficient n-doping and high conductivities. *Adv. Mater.* **33**, 2005946 (2021).
34. Y. Lu, J.-Y. Wang, J. Pei, Achieving efficient n-doping of conjugated polymers by molecular dopants. *Acc. Chem. Res.* **54**, 2871–2883 (2021).
35. S. Luo, T. Wang, M. U. Ocheje, S. Zhang, J. Xu, Z. Qian, X. Gu, G. Xue, S. Rondeau-Gagné, J. Jiang, W. Hu, E. Zhuravlev, D. Zhou, Multiamorphous phases in diketopyrrolopyrrole-based conjugated polymers: From bulk to ultrathin films. *Macromolecules* **53**, 4480–4489 (2020).
36. R. Remy, S. Wei, L. M. Campos, M. E. Mackay, Three-phase morphology of semicrystalline polymer semiconductors: A quantitative analysis. *ACS Macro Lett.* **4**, 1051–1055 (2015).
37. Y.-C. He, K.-F. Xie, Y.-H. Wang, D.-S. Zhou, W.-B. Hu, Characterization of polymer crystallization kinetics *via* fast-scanning chip-calorimetry. *Acta Phys. Chim. Sin.* **36**, 1905081 (2020).
38. Z.-F. Yao, Z.-Y. Wang, H.-T. Wu, Y. Lu, Q.-Y. Li, L. Zou, J.-Y. Wang, J. Pei, Ordered solid-state microstructures of conjugated polymers arising from solution-state aggregation. *Angew. Chem. Int. Ed.* **59**, 17467–17471 (2020).
39. K. P. Pernstich, B. Roessner, B. Batlogg, Field-effect-modulated Seebeck coefficient in organic semiconductors. *Nat. Mater.* **7**, 321–325 (2008).
40. G. J. Snyder, E. S. Toberer, Complex thermoelectric materials. *Nat. Mater.* **7**, 105–114 (2008).
41. H. T. Yi, Y. N. Gartstein, V. Podzorov, Charge carrier coherence and Hall effect in organic semiconductors. *Sci. Rep.* **6**, 23650 (2016).
42. C.-Y. Yang, Y.-F. Ding, D. Huang, J. Wang, Z.-F. Yao, C.-X. Huang, Y. Lu, H.-I. Un, F.-D. Zhuang, J.-H. Dou, C. Di, D. Zhu, J.-Y. Wang, T. Lei, J. Pei, A thermally activated and highly miscible dopant for n-type organic thermoelectrics. *Nat. Commun.* **11**, 3292 (2020).
43. C.-Y. Yang, M.-A. Stoeckel, T.-P. Ruoko, H.-Y. Wu, X. Liu, N. B. Kolhe, Z. Wu, Y. Puttisong, C. Musumeci, M. Massetti, H. Sun, K. Xu, D. Tu, W. M. Chen, H. Y. Woo, M. Fahlman, S. A. Jenekhe, M. Berggren, S. Fabiano, A high-conductivity n-type polymeric ink for printed electronics. *Nat. Commun.* **12**, 2354 (2021).
44. R. R. Søndergaard, M. Hösel, N. Espinosa, M. Jørgensen, F. C. Krebs, Practical evaluation of organic polymer thermoelectrics by large-area R2R processing on flexible substrates. *Energy Sci. Eng.* **1**, 81–88 (2013).
45. Y. Du, K. Cai, S. Chen, H. Wang, S. Z. Shen, R. Donelson, T. Lin, Thermoelectric fabrics: Toward power generating clothing. *Sci. Rep.* **5**, 6411 (2015).

46. Q. Wei, M. Mukaida, K. Kirihara, Y. Naitoha, T. Ishidaa, Polymer thermoelectric modules screen-printed on paper. *RSC Adv.* **4**, 28802–28806 (2014).
47. N. Kim, S. Lienemann, I. Petsagkourakis, D. A. Mengistie, S. Kee, T. Ederth, V. Gueskine, P. Leclère, R. Lazzaroni, X. Crispin, Elastic conducting polymer composites in thermoelectric modules. *Nat. Commun.* **11**, 1424 (2020).
48. F. Jiao, C. Di, Y. Sun, P. Sheng, W. Xu, D. Zhu, Inkjet-printed flexible organic thin-film thermoelectric devices based on p- and n-type poly(metal 1,1,2,2-ethenetetrathiolate)s/polymer composites through ball-milling. *Philos. T. R. Soc. A* **372**, 20130008 (2014).
49. P. Wei, J. H. Oh, G. Dong, Z. Bao, Use of a 1H-benzoimidazole derivative as an n-type dopant and to enable air-stable solution-processed n-channel organic thin-film transistors. *J. Am. Chem. Soc.* **132**, 8852–8853 (2010).
50. M. J. Frisch, G. W. Trucks, H. B. Schlegel, G. E. Scuseria, M. A. Robb, J. R. Cheeseman, G. Scalmani, V. Barone, B. Mennucci, G. A. Petersson, H. Nakatsuji, M. Caricato, X. Li, H. P. Hratchian, A. F. Izmaylov, J. Bloino, G. Zheng, J. L. Sonnenberg, M. Hada, M. Ehara, K. Toyota, R. Fukuda, J. Hasegawa, M. Ishida, T. Nakajima, Y. Honda, O. Kitao, H. Nakai, T. Vreven, J. A. Montgomery Jr., J. E. Peralta, F. Ogliaro, M. Bearpark, J. J. Heyd, E. Brothers, K. N. Kudin, V. N. Staroverov, T. Keith, R. Kobayashi, J. Normand, K. Raghavachari, A. Rendell, J. C. Burant, S. S. Iyengar, J. Tomasi, M. Cossi, N. Rega, J. M. Millam, M. Klene, J. E. Knox, J. B. Cross, V. Bakken, C. Adamo, J. Jaramillo, R. Gomperts, R. E. Stratmann, O. Yazyev, A. J. Austin, R. Cammi, C. Pomelli, J. W. Ochterski, R. L. Martin, K. Morokuma, V. G. Zakrzewski, G. A. Voth, P. Salvador, J. J. Dannenberg, S. Dapprich, A. D. Daniels, O. Farkas, J. B. Foresman, J. V. Ortiz, J. Cioslowski, D. J. Fox, *Gaussian 09, Revision C.01* (Gaussian, Inc., 2010).

Acknowledgments: We thank J. Zhang and Y. Zhao from Peking University for Raman measurements and S. Gao and Y.-H. Fang from Peking University for EPR measurements. **Funding:** This work is supported by the National Key R&D Program of China (2017YFA0204701) and the National Natural Science Foundation of China (22020102001 and 21790360). H.S. thanks the Royal Society for support through a Research Professorship (RP\R1\201082), and H.-I.U. thanks the Engineering and Physical Sciences Research Council (EPSRC) for funding (EP/S030662/1). S.J.Z. acknowledges support from the Polish National Agency for Academic Exchange within the Bekker program (grant no. PPN/BEK/2020/1/00264/U/00001). **Author contributions:** Conceptualization: Z.-D.Y., Y.L., Z.-F.Y., H.S., and J.P. Methodology: Z.-D.Y., Y.L., Z.-Y.W., H.-I.U., and S.J.Z. Investigation: Z.-D.Y., H.-I.U., H.-Y.Y., and Y.C. Supervision: J.P., H.S., J.-Y.W., W.-B.H., Y.-C.H., and K.-F.X. Writing—original draft: Z.-D.Y. Writing—review and editing: Y.L., H.-I.U., J.-Y.W., W.-B.H., H.S., and J.P. **Competing interests:** The authors declare that they have no competing interests. **Data and materials availability:** All data needed to evaluate the conclusions in the paper are present in the paper and/or the Supplementary Materials.

Submitted 15 October 2022
Accepted 25 January 2023
Published 24 February 2023
10.1126/sciadv.adf3495